

Using magnetic levitation for 2D and 3D self-assembly of cubic silicon macroparticles

Léon A. Woldering¹, Auke J. Been¹, Laurens Alink¹, and Leon Abelmann^{*1,2}

¹ MESA + Institute for Nanotechnology, University of Twente, P.O. Box 217, 7500AE Enschede, The Netherlands

² Korea Institute of Science and Technology, Campus E7 1, 66123 Saarbrücken, Germany

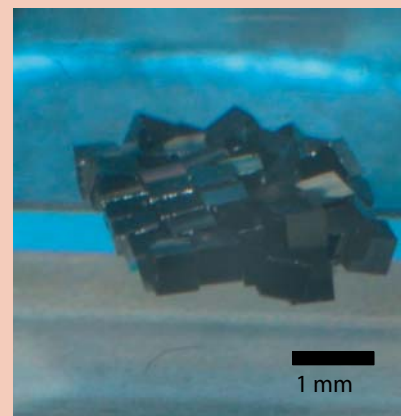
Received 17 August 2015, revised 1 November 2015, accepted 9 November 2015

Published online 20 November 2015

Keywords self-assembly, magnetic levitation, hydrophobic interaction, silicon particles

* Corresponding author: e-mail l.abelmann@kist-europe.de

Today's micro- and nano-fabrication is essentially two-dimensional, with very limited possibilities of accessing the third dimension. The most viable way to mass-fabricate functional structures at the nano-scale, such as electronics or MEMS, with equal feature sizes in all directions, is by three-dimensional self-assembly. Up to now, three-dimensional self-assembly has mainly been restricted to crystals of polymer spheres. We report on two- and three-dimensional self-assembly of silicon cubes, levitated in a paramagnetic fluid. We demonstrate the benefits of templating and study the effect of a change in hydrophilicity of the cubes. These experiments bring us one step closer to three-dimensional self-assembly of anisotropic, semiconducting units, which is a crucial milestone in overcoming the scaling limits imposed by contemporary 2D microfabrication.



Levitated assembly of silicon cubes.

© 2016 WILEY-VCH Verlag GmbH & Co. KGaA, Weinheim

1 Introduction Self-assembly is the process in which units such as atoms, molecules, colloidal or microfabricated particles spontaneously form organized structures [1]. The final shape and properties of the resulting structure is entirely determined by the properties of the individual units, and not by external (human) direction.

Self-assembly occurs at all length scales, from the tiniest molecules to entire galaxies [2]. In this paper, we study the three-dimensional self-assembly of anisotropic silicon particles as a fabrication technique for 3D silicon micro-machining. Self-assembly of microfabricated objects in two dimensions has received wide attention with promising results [3, 4] and very complex shapes [5]. The transition to three dimensions is of technological importance for complex structures such as photonic band gap materials [6,

7], metamaterials fabricated from cubic building blocks [8], three-dimensional electrical networks [9] and 3D cross-point architectures for computer memories [10]. Processes for 3D silicon microfabrication are necessary in order to overcome the scaling limits imposed by 2D micro-fabrication [11, 12].

For self-assembly, four elements are critical: the characteristics of the individual units, the driving forces which bind the units, the disturbing forces which allow the units to find their optimal position, and the environment in which the self-assembly takes place [1]. Organized structures are obtained when these four elements are properly tuned. For submicrometer sized particles, the gravitational force is small compared to drag forces and sedimentation of particles is slow [6]. However, in our research we use

particles of several hundred μm . At these length scales, sedimentation takes place too rapidly, and has an undesired effect on the outcome of the self-assembly experiments. Therefore there is a need to counteract gravity in these systems. To this end we employ the magneto-Archimedes levitation [13] in a paramagnetic fluid, sometimes also called diamagnetic levitation [14–16]. We prefer the term magneto-Archimedes, since strictly speaking the levitated objects do not have to be diamagnetic, as long as they are less paramagnetic than the surrounding fluid. The magneto-Archimedes effect also provides a driving force pushing the particles towards each other [17, 18].

Magnetic forces are increasingly used in self-assembly. For instance, assembly was performed using magnetic nanoparticle fluids [19], magnetite nanocubes have been self-assembled into helical superstructures [20], a macro-scale Zeeman slower was fabricated from permanent magnets [21], and colloidal assembly was directed by magnetic moulds [22].

Here we report on the 2D and 3D self-assembly of levitated silicon macrocubes. Since the magneto-Archimedes driving force in our system is axi-symmetric, we expect the target structures to be cubic closed packed disc-like (2D case) or ellipsoid-like (3D case) structures, built from the constituent macrocubes. The submillimeter particles were levitated in a paramagnetic fluid. These particles have a much higher density than commonly used [17, 18]. Early results indicated that the levitated 3D self-assembly of these macrocubes is very challenging [23]. Therefore, in order to increase the quality of the resulting 3D crystals, the particles were made less hydrophilic. This reduction in hydrophilicity introduces additional binding forces between the particles that are in contact, as was demonstrated by means of the self-assembly of hydrophobic silver nanocubes [24] and other anisotropic shapes [25].

We demonstrate successful 2D and 3D templated self-assembly, as well as the 3D levitated self-assembly of silicon macrocubes. These results are the first ever 3D self-assembly of silicon particles with an anisotropic shape by means of magnetic levitation. This method is a promising route towards 3D micromachining of silicon aided by self-assembly.

2 Experimental The self-assembly experiments were performed in a home-built setup, fabricated from aluminum, schematically depicted in Fig. 1(A). In this setup a cuvette filled with a paramagnetic liquid and up to 54 diamagnetic silicon macrocubes was positioned between two NdFeB magnets. These magnets were obtained by stacking 5 smaller cylindrical magnets, resulting in a stack with a total length of $l = 35$ mm and a radius of $r = 12.5$ mm. The magnetic field strength at the edge of the magnets was measured with a Gauss meter to be 1.25 T. By placing these stacks of magnets so that similar poles face each other, a magnetic field gradient is obtained in the cuvette. The gradient and point of zero field was adjusted by

changing the distance between the magnets from 14 mm to 22 mm by raising magnet 1.

The silicon particles are pushed towards a position on the central axis between the two magnets as a result of the magnetic field gradient inside the paramagnetic medium. This is the position where the magnitude of the magnetic field is lowest¹. Since all particles are forced towards this central region, an effective pressure exists that keeps the particles in close contact.

By changing the separation h between the two magnets, the magnetic field gradient can be altered, which aids attempts to obtain the target structures. The paramagnetic fluid used is a 2M solution of GdCl_3 (Sigma Aldrich G7532, gadolinium(III)chloride hexahydrate 99%) in demineralized water. The relatively strong susceptibility of this fluid enhances the susceptibility contrast between the diamagnetic macrocubes and the paramagnetic liquid environment.

In order to introduce vibrations into the system, one end of the cuvette is pressed against a piezo-actuator (FPA-0150E-S-0518-150-SS-1M3 FlexFrame PiezoActuator, Dynamic Structures & Materials, LLC).

The electric capacity of the piezo-element is 1.8 μF . A spring ensures that the cuvette is kept in position while the piezo-element is actuated. The actuation frequency and amplitude are generated by means of a waveform generator (Agilent A33220A), which is connected to a $10\times$ high voltage amplifier (SyLAB LM3325). Typically the piezo-element was actuated for 30 minutes. Care was taken to prevent strong oscillatory fluid flows, which typically results in an undesired alignment of particles at the nodes of the resulting standing waves. We determined an actuation frequency of 300 Hz with a peak to peak voltage of 130 V to be optimal for self-assembly. From this voltage and the capacity of the piezo-element, we can estimate that the upper limit in the disturbing energy in the system is in the order of 15 mJ.

The macrocubes were diced from a double-sided polished silicon wafer (p-type, $\langle 100 \rangle$, resistivity = 5–10 $\Omega\text{ cm}$). The dicing procedure was optimized in order to make sure that the particles be as cubic as possible and that the diced surfaces be as smooth as possible. To obtain the cubes, first the average thickness of the wafer was determined around the edge of the wafer by a micrometer caliper to be 525 μm . The manufacturer specifies a thickness variation over the entire wafer of less than 5 μm . Subsequently, the wafer was diced so that edges were obtained with lengths equal to the measured average thickness of the wafer. For dicing, we employed a Loadpoint Micro Ace 3 dicing saw, equipped with an F1230 blade. The blade was operated at 32000 rpm at a feed rate of 1 mm/s. Any residual dicing foil was removed using a piranha solution ($\text{H}_2\text{SO}_4(\text{conc}) : \text{H}_2\text{O}_2(30\%) = 4 : 1$, temperature = 100 $^\circ\text{C}$, 10 min), followed by rinsing. The particles were stored in

¹ The actual position of assembly is slightly lower due to gravity.

demineralized water. Inspection by scanning electron microscopy (FEI Quanta 450) confirmed that the particle size was as designed within measurement error ($519 \pm 10 \mu\text{m}$).

In order to optimize the dicing process for flatness of the cubes, the morphology of the resulting surface was analysed by means of scanning electron micrographs (FEI Quanta 450). Atomic force microscopy (AFM, Dimension 3100) on a face of a single particle resulted in a RMS roughness of 12.6 nm over a $10 \mu\text{m}$ scan range, with a peak-peak value of 460 nm.

Due to the native surface oxide, the water wets the silicon cubes completely (contact angle of 0°). Some of the cubes were made less hydrophilic by means of chemical functionalization with hexamethyldisilazane (HMDS) [26, 27].

To begin with, the macrocubes were heated on a hot-plate at $70 \pm 20^\circ\text{C}$ to remove any adsorbed water from the surface. Subsequently, the particles were immersed in pure HMDS (BASF, VLSI Selectipur). The surface reaction between the silicon and HMDS was allowed to proceed for one minute while stirring, after which the suspension was poured on top of a Whatman general purpose filter paper. The residual HMDS was quickly removed by rinsing the particles with excess acetone (VWR Chemicals, Technical grade, 99%) and isopropyl alcohol (Merck Millipore, for analysis, 99.8%). The macrocubes were dried in air.

This chemical reaction was also performed on a whole, unprocessed wafer. This wafer allowed the contact angle of a droplet of water on the silicon surface to be measured before and after the reaction, in order to characterize the change in hydrophilicity. The contact angles were measured using a Metrology Dataphysics OCA-20. After the one minute HMDS treatment, the surface became less hydrophilic with a contact angle of 53° .

The macrocubes were used for several 2D and 3D self-assembly experiments. In this paper we report 4 different experiments:

- Measuring the levitation height of single macrocubes as a function of the magnet separation h .
- Templated 2D self-assembly of macrocubes on the bottom of the cuvette.
- Templated 3D self-assembly of macrocubes on the bottom of the cuvette.
- Levitated 3D self-assembly of macrocubes.

Typically, around 54 macrocubes were used for the self-assembly experiments.

The levitation heights of single silicon macrocubes were measured by means of non-magnetic, synthetic calipers (WIHA, Vernier Calipers #41103). Two cameras were used to observe the self-assembly experiments: a Dino-lite pro USB microscope and a Nikon 1 J2 compact flash camera. The latter was equipped with a Macro-Switar 1:1.9 CMT lens (focal length = 75 mm) and an 85 mm extension tube. The results were stored as photographs, see for example Figs. 2 and 4, or as videos (see Supporting Information).

3 Results and discussion

3.1 Levitation of single macrocubes Single, non-surface treated macrocubes were levitated in the paramagnetic fluid with different magnet separations. The resulting measured particle levitation heights are plotted in Fig. 1(B). The separation distance h between the two cylindrical magnets was changed by raising magnet 1. As a result, the point of zero field is raised as well. In this way levitation heights over 4 mm could be achieved. The measured heights are compared to the expected values based on a magnetostatic model, which takes into account the distribution of magnetic field energy throughout the area of interest. The model neglects magnetic interparticle interactions and assumes that the particles are small, so the force density is constant over the volume of the particle. Details can be

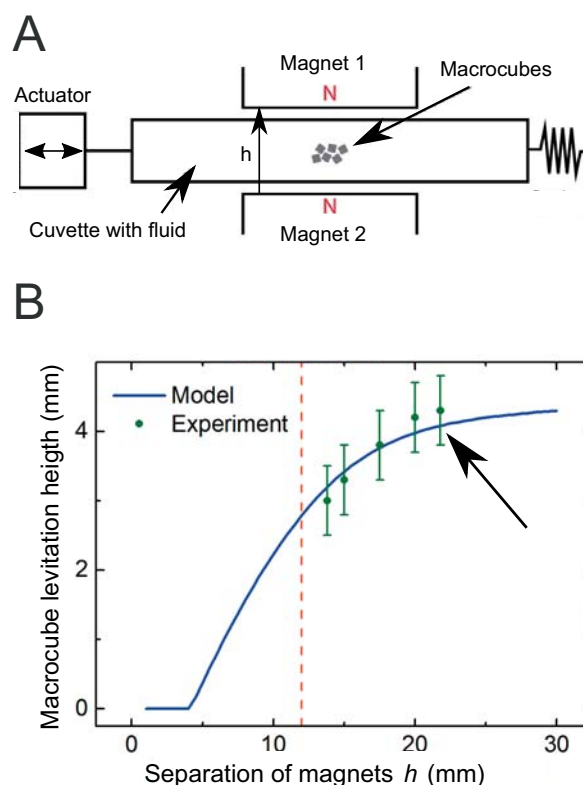


Figure 1 (A) Schematic illustration of the home-built setup. Silicon macrocubes are introduced to a cuvette that contains a paramagnetic liquid. The cuvette is positioned between two magnets, which are placed with similar poles facing. The resulting magnetic field gradient causes the particles to be forced towards a central region between the two magnets, labelled Magnet 1 and Magnet 2. A piezo-actuator introduces vibrations into the cuvette, which allows self-assembly to occur. Cameras were used to visualize the self-assembly process and the resulting arrays of particles. (B) Measured levitation height (green dots) of a single silicon macrocube as a function of magnet separation h . The measured data are compared to values expected based on our theoretical model (solid line). The dashed line is the minimum separation of the magnets, as dictated by the dimensions of the cuvette. The maximum separation is indicated by the arrow.

found in Appendix A. The theoretical and measured values are found to be in excellent agreement, see Fig. 1(B), which confirms that our model provides a good description of the experiment.

3.2 Two-dimensional self-assembly Two-dimensional self-assembly of macrocubes was performed on the bottom of the cuvette. The cuvette acts as a template and makes sure that all the particles are positioned in the same plane. Figure 2(A) is a photograph of the macrocubes on the bottom of the cuvette before self-assembly. It is apparent that the particles are randomly positioned, resulting in a high amount of disorder. Figure 2(B) is a photograph of the macrocubes after self-assembly for 20 minutes. The generated vibrations allow the particles to optimize their position in the magnetic field, that is, find those positions where the total energy of the array is as low as possible. In the final array, the particles have aligned themselves neatly next to each other, resulting in a square distribution of the macrocubes, which is the target configuration. Some deviations from the ideal square distribution are observable.

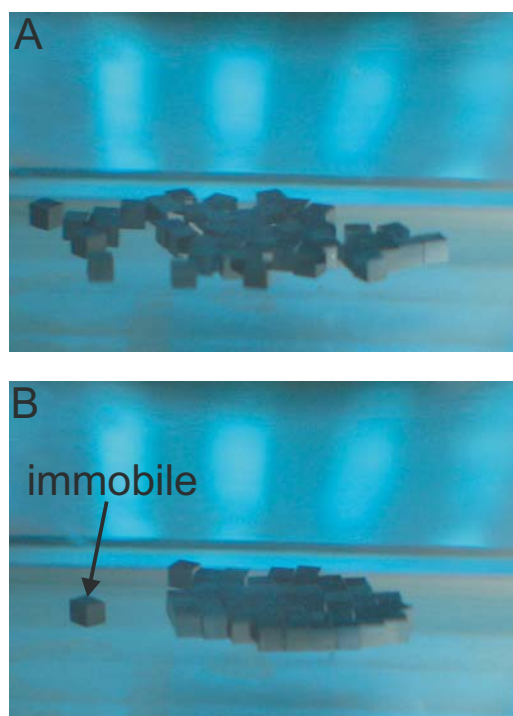


Figure 2 (A) Collection of randomly distributed silicon macrocubes before 2D self-assembly. The particles are lying on the bottom of the cuvette, which acts as a template. The macrocubes are surface treated to make them less hydrophilic and have edges of $525 \pm 10 \mu\text{m}$. (B) Array of silicon cubes after self-assembling for 20 minutes. During this time the piezo-actuator was operated in order to introduce a vibration to the system. The particles are aligned next to each other in a square distribution. Deviations from the ideal configuration are observable. A video of the self-assembly process can be found in the Supporting Information (video 1, SA_2D_Templated).

The theoretical model employed in the previous section is also used to analyse the magnetic energy of these templated 2D arrays. In this case the model is modified slightly in order to take the rotational orientation of the cubes into account. Details can be found in Appendix B. We have analysed the magnetic energy of the 2D array of macrocubes at intervals of 50 seconds for a 1500 seconds self-assembly experiment, see Fig. 3(A). In these photographs, the position of each individual macrocube was determined manually with the aid of a MATLAB script that transforms the perspective (see Appendix C). Subsequently the known distribution of the magnetic field energy in the cuvette was used to calculate the cumulative energy of the array. The calculated energy is given with respect to the value of the magnetic energies of a square configuration, see insets in Fig. 3(A). At time < 600 seconds, a rapid de-

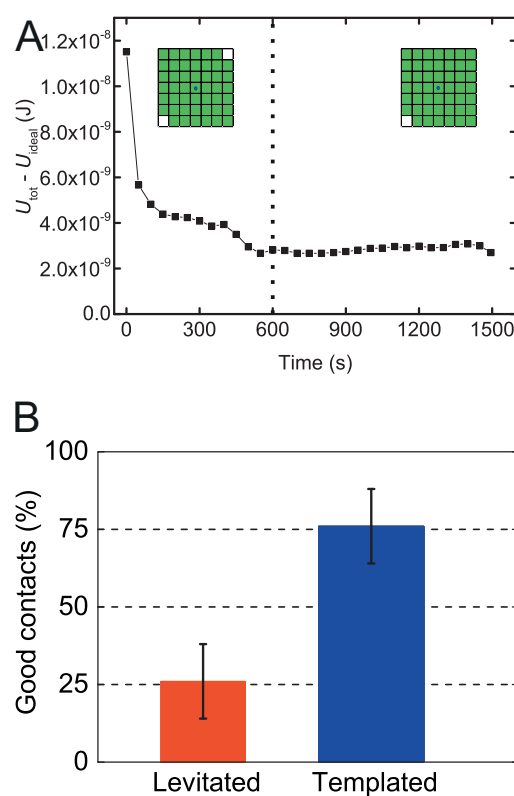


Figure 3 (A) Difference between calculated energy of observed 2D arrays and of target configuration versus time. The energy difference decreases with time, indicative of energy minimization. After 600 seconds, the energy difference remains at around $U = 3 \text{ nJ}$. The insets show the square target configurations for the number of cubes in the field of view. There are some missing cubes at the corners of the structures, since the number of macrocubes was insufficient for full squares. At 600 seconds an additional cube entered, which is reflected in the target structure. (B) Number of good contacts in arrays resulting from templated self- and levitated self-assembly of surface treated macrocubes. The vertical bars depict the standard deviation of the measurements. The levitated and templated experiments were repeated 12, respectively 3 times.

crease of the energy difference between the actual and the square array is observed. From this result we surmise that energy minimization is indeed achieved when operating the piezo-actuator. This means that there is a good balance between the vibrational energy in the system and the energy forcing the macrocubes together. Consequently, we confirm that this setup is very suitable for this self-assembly process. After 600 seconds, the energy difference levels off at a value of around $U = 3$ nJ. Since the energy difference remains constant at a value which is non-zero, it is apparent that the lowest possible energy is not obtained. The optimal configuration has lower energy. A possible explanation is that the introduced vibrations are still too energetic. In this respect, it is tempting to compare the energy levels with the energy pumped into the system by the piezo. From the upper limit of 15 mJ provided by the power source, a fraction is taken up by the array of particles. If we assume this fraction is the volume of the particles to the entire volume of the system (about 15×10^3), the energy a single particle can absorb is about 1 μ J. Since this value is a factor of thousand above the observed energy levels, this approach is probably too naive. Other attempts to estimate the disturbing energy in the system from macroscopic inputs, such as the velocity of the piezo, lead to much too high values as well.

3.3 Three-dimensional self-assembly Self-assembly in three-dimensions was demonstrated by means of two examples: (i) templated, see Fig. 4(A) and (ii) levitating, see Fig. 4(B). As a template, again the bottom of the cuvette was used as in the 2D situation, but magnet 1 was not lowered as much. In the levitated case, the macrocubes were made less hydrophilic, to enhance the interaction.

In both cases, the target structure is a large 3D perfect primitive cubic crystal built from individual macrocubes. In both cases we find that many of the macrocubes are nicely aligned with each other and that the structure obtained closely matches the target structure. The result for the templated case appears to be much better than the levitated case, as expected. This result is understandable from the intuitive argument that in the templated case, pre-organization along one of the plane directions in the crystal is provided.

To quantify these results, we used photographs of the resulting 3D structures, similar to those in Fig. 4, to determine the percentage of observable good contacts between particles as a ratio with the total number of observable contacts. The six faces of each macrocube that could be observed were assessed. Contacts with an overlap of more than 95% were rated as good. All other contacts are rejected, but counted. Furthermore, in the case of rotational misalignment, the contact is also rejected as bad. Faces that cannot be seen are not counted. For both types of 3D self-assembly, the relative number of good bonds was determined and compared in Fig. 3(B).

For the templated case, we find around 75% good contacts, compared to around 25% for the levitated experiment.

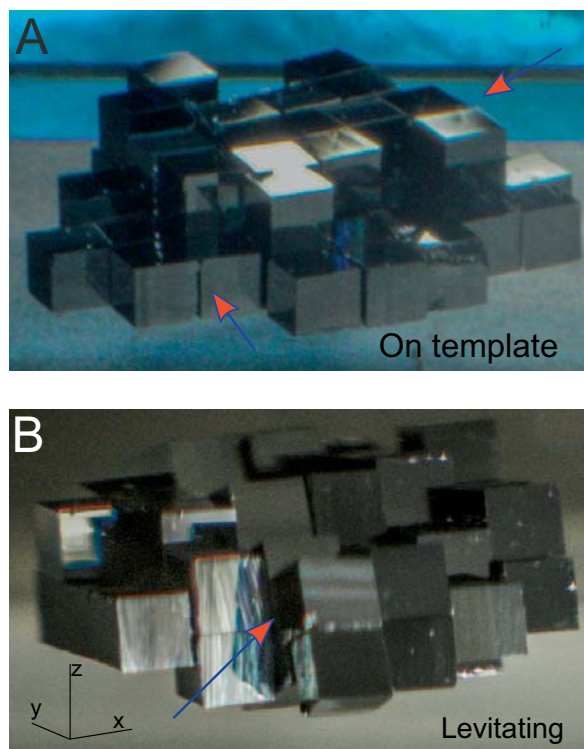


Figure 4 (A) Photograph of the resulting array after 3D self-assembly in a paramagnetic liquid of hydrophilic silicon cubes on a template. The template is formed by the bottom of the cuvette. The macrocubes are successfully organized in a structure that closely resembles the target 3D cubic crystal, see for example the positions at the arrows. (B) Photograph of the resulting array after 3D self-assembly of levitating surface treated silicon cubes. The structure is a good match to the target cubic crystal, however small structural mismatches are identifiable, see for example the arrow. In particular, rotational and positional alignment errors are visible in between separate crystal planes. A video of the self-assembly process can be found in the Supporting Information (video 2, SA_3D_Templated).

This result confirms the qualitative observation that the templated results are better than the levitated self-assembly.

In the levitated case, when the macrocubes are made less hydrophilic the number of faces that had no observable rotational misalignment appeared to increase. The surface treatment, however, seems to have no significant effect on the number of good contacts. The effect of a change in hydrophilicity requires more research before definite conclusions can be drawn.

In the photograph in Fig. 4(B) we find deviations from the perfect primitive cubic crystal structure. There appear to be planes of cubes aligned vertically (yz -planes), that are rotated with respect to each other (around the x -axis). We speculate that this is related to the anisotropy in the disturbing energy, caused by the fact that the piezo introduces sound waves along the long axis of the cuvette.

One can observe an elongation of the entire assembly in the xy -plane. This effect is due to the shape of the force

field, which is slightly ellipsoidal, with the short axis along the z -direction. This shape can be adjusted by modifying the distance between the magnets.

From these results it is apparent that this method has high potential for 3D self-assembly. We surmise that by tuning the hydrophilicity of the particles and the making the vibrational energy in the system less directional may result in an even closer match with the target structure.

4 Conclusions We have demonstrated two- and three-dimensional self-assembly of anisotropic silicon cubes with edges of 525 μm , treated with HDMS to make them less hydrophilic. To provide a driving force for self-assembly and avoid sedimentation, the cubes were levitated in a paramagnetic GdCl_3 solution. We have shown that the levitation height is controllable up to approximately 4 mm by changing the distance between the two permanent magnets that generate the magnetic field.

A piezo element in our setup provides energy that drives the energy of the system towards a global minimum. For two-dimensional self-assembly, this was demonstrated by calculating the magnetic energy as a function of time.

The use of a non-structured surface as template is beneficial for successful self-assembly. For the 3D experiment, the fraction of cube faces that are fully aligned increases from 25% to 75% after inserting a template. The resulting structure is a good match with the target cubic crystal structure.

Further optimization is expected to be possible by tuning the hydrophilicity of the macrocubes and of the vibrational energy in the system. This method is a promising route towards magnetically driven 3D self-assembly for applications such as 3D photonic bandgap crystals [7] or memory crystals [10].

Supporting Information Additional Supporting Information may be found in the online version of this article at the publishers web-site.

Acknowledgements The authors thank Miko Elwenspoek and Jan Eijkel for inspiring discussions and Remco Sanders and Garud Snoep for helpful assistance. This work was financially supported by a VENI fellowship (Technical Sciences) by the Netherlands Organisation for Scientific Research (NWO) to LAW.

Appendix

A Diamagnetic levitation Diamagnetic materials are repelled from magnetic fields [28], which makes diamagnetic materials perfect for magnetic levitation. The degree to which a material is diamagnetic is measured in the magnetic susceptibility χ . For diamagnetic materials this is a negative number, for paramagnetic materials – materials attracted to magnetic fields – this is a positive number. Strongly diamagnetic materials, like pyrolytic graphite, are easy to levitate [14] in contrast to weakly diamagnetic materials. The challenge to levitate a weakly diamagnetic material, like silicon, can be overcome with a paramagnetic

medium [29]. By surrounding the weakly diamagnetic material with a strongly paramagnetic medium, levitation can be achieved [30]. The paramagnetic medium is attracted to the magnets, pushing the diamagnetic material away: Magnetic levitation is achieved. The forces involved with diamagnetic levitation in a paramagnetic medium are two-fold: On the one hand, there is a buoyant force, depending on the gravity, densities of the two materials, and volume of the diamagnetic particle. On the other hand, there is a magnetic force, which is dependant of the magnetic susceptibilities of the two materials, volume of the diamagnetic particle, and the applied magnetic field. Since both forces are a function of particle volume, the force density can be determined [30]. Assuming that the susceptibility is small, so that the liquid is not saturated, and that the particles is small, so that the force density is more or less constant,

$$\mathbf{F}/V = -(\rho_l - \rho_p) \mathbf{g} - \frac{(\chi_l - \chi_p)}{\mu_0} (\mathbf{B} \cdot \nabla) \mathbf{B}, \quad (1)$$

where \mathbf{F} is the force on the particle, V is its volume, ρ is the density and χ the magnetic susceptibility of particle p and liquid medium l . Vector \mathbf{g} is the gravitational acceleration, μ_0 the vacuum permeability and \mathbf{B} the magnetic field. The density of silicon is $\rho_p = 2329 \text{ kg/m}^3$ [31], the density of a 2 M GdCl_3 solution in water was measured to be $\rho_l = 1459 \text{ kg/m}^3$. The magnetic susceptibility can be calculated for the GdCl_3 solution in water, see Eq. (2) [29].

$$\chi_l = 27.930 \times 10^{-3} \cdot 4\pi \cdot C, \quad (2)$$

where C is the concentration of GdCl_3 in water, in this work 2 M. At these concentrations, the magnetic susceptibility of silicon is negligible ($\chi_p = -3.215 \times 10^{-6}$ [29]).

In order to obtain a stable levitation point, two magnets can be placed close to each other with similar poles facing [32]. To calculate the forces on a particle, the magnetic field needs to be determined. For the calculation of the magnetic field of a single magnet, the Biot–Savart equation was used, see Eq. (3) [28].

$$\mathbf{B}(\mathbf{r}_1) = \frac{\mu_0}{4\pi} \iiint \frac{\mathbf{j}(\mathbf{r}_2) \times \mathbf{r}_{12}}{r_{12}^3} dV_2, \quad (3)$$

where \mathbf{B} is the magnetic field, μ_0 is the permeability of free space, $\mathbf{r}_{12} = \mathbf{r}_1 - \mathbf{r}_2$ is the full displacement vector, \mathbf{j} is the current density in V_2 , and V_2 is the volume of the magnet. To take advantage of the cylinder symmetry (in this work, cylindrical magnets were used), a cylindrical coordinate system is used. In the cylindrical coordinate system r , φ and z are used as coordinate variables. The vectors \mathbf{r}_1 and \mathbf{r}_2 take the form of $\mathbf{r}_1 = [r_1, \varphi_1, z_1]$ and $\mathbf{r}_2 = [r_2, \varphi_2, z_2]$. As indicated in Eq. (3), \mathbf{r}_2 is used for the integration volume, i.e. the magnet. The vector \mathbf{r}_1 is the location at which the magnetic field is calculated. Assuming the magnetisation is constant throughout the volume of the magnet, and using

$\mathbf{j} = \nabla \times \mathbf{M}$ [28], then \mathbf{j} is given by Eq. (4),

$$\mathbf{j} = M_z \delta(r_2 - R) u(z_2) u(L - z_2) \hat{\phi}, \quad (4)$$

where R is the radius of the magnet, L is the length of the magnet, δ is the Dirac delta, u the step function and $\hat{\phi}$ is the unit vector of the ϕ direction. Note that φ_2 can be taken as zero for our axisymmetrical system. The magnetisation of the magnets used in this work was calculated from a magnetic field measurement at the edge of the magnets, and is 1.25 T.

To obtain a two magnet model, the field of the second magnet is shifted by $z = L + h$ and superimposed on the field of the first magnet, where h is the separation between the magnets.

To avoid elliptical integrals [33], implementation of Eq. (3) includes a discrete summation of the integral over φ . All analytical calculations were performed using MATLAB². The analytical model was verified with finite element method (FEM) simulations using COMSOL³; the FEM model agrees with the analytical calculations within 0.3 in the region between the magnets. The analytical calculations of the magnetic field were used to model the levitation height as in Eq. (1).

B Energy of assembly To calculate the magnetostatic forces on the particles and the energy of their ensemble, we derive an approximate solution of the quasi-static, no-current, Maxwell equations. The liquid and the particles are modeled as linear permeable regions. Their permeabilities are respectively $\mu_l = \mu_0 \cdot (1 + \chi_l)$ and $\mu_p = \mu_0 \cdot (1 + \chi_p)$, where the χ 's are magnetic susceptibilities and μ_0 the vacuum permeability. The applied magnetic field is due to exterior sources. We define $-\nabla\varphi = \mathbf{H}$, $\mathbf{B} = \mu(\mathbf{H} + \mathbf{m})$, so $\nabla \cdot \mathbf{H} = -\nabla \cdot \mathbf{m}$. It is convenient to take $\mu = \mu_l$. Then the induced magnetisation $\mathbf{m} = 0$ in the liquid and $\mathbf{m} = (\chi_p - \chi_l) \mu_0 / \mu_l \mathbf{H}$ in the particle.

Our main approximation concerns the boundary conditions imposed on φ at the interface between regions with different permeability. These conditions are: (I) φ is continuous over the interface and (II) $\mu_l \frac{\partial \varphi}{\partial \mathbf{n}} \Big|_l = \mu_p \frac{\partial \varphi}{\partial \mathbf{n}} \Big|_p$, where \mathbf{n} is the, say, outer surface normal. For small susceptibilities ($\chi \ll 1$), we can violate condition (II) a bit and take $\mu_p \frac{\partial \varphi}{\partial \mathbf{n}} \Big|_p \approx \mu_l \frac{\partial \varphi}{\partial \mathbf{n}} \Big|_l$, so $\frac{\partial \varphi}{\partial \mathbf{n}}$ is continuous. Then \mathbf{H} is determined solely by the free-space field of the exterior sources. Consequently, there is no inter-particle interaction. Next to this, we will use $\mu_l \approx \mu_0$.

With these approximations, the energy of a particle in the susceptible liquid background is then given by

$$U = -\frac{1}{2} \int \mathbf{m} \cdot \mathbf{B} \, dV, \quad (5)$$

$$U = -\frac{1}{2\mu_0} \int_{V_p} (\chi_p - \chi_l) |\mathbf{B}|^2 \, dV, \quad (6)$$

where V_p is the volume of the particle, and the field $\mathbf{B} = \mu_0 \mathbf{H}$ is given by the free-space/vacuum field of the sources (i.e. the static magnets). Upon differentiation with respect to the particle position we obtain the force on the particle

$$\mathbf{F} = -\nabla U, \quad (7)$$

$$\mathbf{F} = \frac{1}{2\mu_0} \int (\chi_p - \chi_l) (\nabla |\mathbf{B}|^2) \, dV, \quad (8)$$

or

$$\mathbf{F} = \frac{1}{\mu_0} \int_{V_p} (\chi_p - \chi_l) (\mathbf{B} \cdot \nabla) \mathbf{B} \, dV, \quad (9)$$

where we used $\nabla \times \mathbf{B} = 0$ (which holds, as \mathbf{B} is given by a free-space field). For small gradients of \mathbf{B} over the particle volume, the force is well represented by the force density

$$\mathbf{F}/V = \frac{1}{\mu_0} (\chi_p - \chi_l) (\mathbf{B} \cdot \nabla) \mathbf{B}. \quad (10)$$

This is a familiar expression [30], applicable in case of small particles and small susceptibilities.

Equation (6) has been used to calculate the energy of a system of particles. Numerically, $|\mathbf{B}|^2$ was calculated/tabulated once (as function of radial distance and z) at high resolution. We used this table together with linear interpolation to integrate over the particle volume by means of Riemann summation, taking the position and orientation (i.e. rotation) of the particle into account. The energy of the ensemble is the sum of the energies of the individual particles.

C Perspective transformation To calculate the energy of the particles in the 2D self-assembly process, we determined their position and orientation in photographs (e.g. Fig. 2). For this purpose it is convenient to have a top-view of the particles. We applied a perspective transform to attain this view.

For the perspective transformation we consider a matrix, A , that maps 2D world coordinates (x, y) to image/pixel coordinates (i, j) [34]. A general linear transformation is given by

$$\begin{bmatrix} x \\ y \\ 1 \end{bmatrix} = A \cdot \begin{bmatrix} i \\ j \\ 1 \end{bmatrix}, \quad (11)$$

² MATLAB R2013a, MathWorks, Natick, US.

³ COMSOL 4.3, COMSOL BV, Zoetermeer, The Netherlands.

with

$$A = \begin{bmatrix} a_{xi} & a_{xj} & a_{x1} \\ a_{yi} & a_{yj} & a_{y1} \\ a_{1i} & a_{1j} & a_{11} \end{bmatrix}. \quad (12)$$

Such transformation matrices are routinely inverted in camera calibration methods that employ a calibration grid (e.g. checkerboard pattern) with known world coordinates [34]. Here, we do not have such a fixed grid. However, we know the dimensions of the cubical particles. For instance, the vertices of the top face of a cube are related by

$$\begin{aligned} \mathbf{p}_2 - \mathbf{p}_1 &= \mathbf{u}, \\ \mathbf{p}_3 - \mathbf{p}_4 &= \mathbf{u}, \\ \mathbf{p}_3 - \mathbf{p}_2 &= \mathbf{v}, \\ \mathbf{p}_4 - \mathbf{p}_1 &= \mathbf{v}, \end{aligned} \quad (13)$$

where $\mathbf{p}_{1...4}$ are the vertices oriented in a counterclockwise fashion. Since the top face of a particle is square in real world coordinates, the edges are orthogonal and related via

$$\begin{aligned} \mathbf{u} &= \begin{bmatrix} u_x \\ u_y \end{bmatrix}, \\ \mathbf{v} &= \begin{bmatrix} -u_y \\ u_x \end{bmatrix}. \end{aligned} \quad (14)$$

Substituting (11) and (14) in (13) results a set of equations in terms of (I) the elements of matrix A (i.e. the a 's),

(II) the M pairs of diagonal coordinates ($u_{x,m}$ and $u_{y,m}$) and (III) the $M \times 4$ pairs of vertex coordinates in the image ($i_{1...4,m}$ and $j_{1...4,m}$). Unknown are (I) and (II), known are (III). Additionally, we defined the origin in the photograph as the central pixel (resulting in $a_{x1} = a_{y1} = 0$) and we define the x -axis by

$$a_{xi}\Delta i_0 + a_{xy}\Delta j_0 - 1 = 0, \quad (15)$$

where $(\Delta i_0, \Delta j_0)$ is the vector in the image that corresponds to the unit x -axis. The matrix elements of A are solved by minimizing the mean squared error in (13) and (15). For this, the vertex coordinates were determined manually (i.e. by eye) in a photograph. For the actual transformation we used the `imtransform` function of the MATLAB image processing toolbox. This transformation was applied to entire photographs, however, only the pixels that correspond to positions in the plane of the top faces of the cubes are correctly transformed. Figure 5 shows an example of the perspective transformation.

References

- [1] J. Pelesko, *Self Assembly: The Science of Things That Put Themselves Together* (Chapman & Hall, Boca Raton, 2007).
- [2] G. Whitesides and B. Grzybowski, *Science* **295**, 2418–2421 (2002).
- [3] A. Tkachenko and J. Q. Lu, *J. Magn. Magn. Mater.* **385**, 286–291 (2015).
- [4] J. Goldowsky, M. Mastrangeli, L. Jacot-Descombes, M. Gullo, G. Mermoud, J. Brugger, A. Martinoli, B. Nelson, and H. Knapp, *J. Micromech. Microeng.* **23**(12), 125026 (2013).
- [5] M. Mastrangeli, A. Martinoli, and J. Brugger, *Microelectron. Eng.* **124**, 1–7 (2014), cited By 0.
- [6] Y. Vlasov, X. Z. Bo, J. Sturm, and D. Norris, *Nature* **414**, 289–293 (2001).
- [7] L. Woldering, L. Abelmann, and M. Elwenspoek, *J. Appl. Phys.* **110**, 043107-1–043107-8 (2011).
- [8] P. Belov, A. Slobozhanyuk, D. Filinov, I. Yagupov, P. Kapitanova, C. Simovski, M. Lapine, and Y. Kivshar, *Appl. Phys. Lett.* **103**, 211903-1–211903-4 (2013).
- [9] D. Gracias, J. Tien, T. Breen, C. Hsu, and G. Whitesides, *Science* **289**, 1170–1172 (2000).
- [10] L. Abelmann, N. Tas, E. Berenschot, and M. Elwenspoek, *Micromachines* **1**(1), 1–18 (2010).
- [11] D. Park, K. Kim, and B. I. Ryu, *Proc. 7th Int. Conf. on Solid-State and Integrated Circuits Technology*, pp. 35–40 (2004).
- [12] M. Elwenspoek, L. Abelmann, E. Berenschot, J. van Honschoten, H. Jansen, and N. Tas, *J. Micromech. Microeng.* **20**, 064001-1–064001-28 (2010).
- [13] Y. Ikezoe, N. Hirota, J. Nakagawa, and K. Kitazawa, *Nature* **393**, 749–750 (1998).
- [14] R. Pelrine, *Amer. Sci.* **92**(5), 428–435 (2004).
- [15] J. Hennek, A. Nemiroski, A. Subramaniam, D. Bwambok, D. Yang, D. Harburg, S. Tricard, A. Ellerbee, and G. Whitesides, *Adv. Mater.* **27**(9), 1587–1592 (2015).

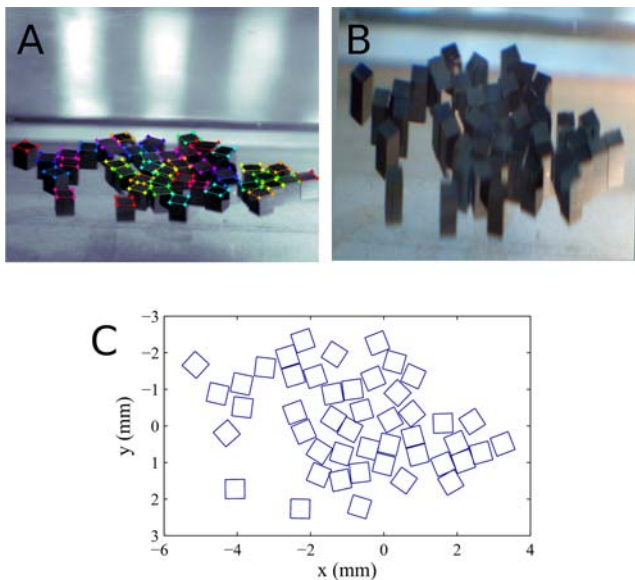


Figure 5 Example of the perspective transformation. (A) A raw photograph with manually detected vertices of the top faces of the particles; (B) the image after perspective transformation and color enhancement; the top faces have been transformed into squares. (C) Positions and orientations of the particles, which were manually detected in the transformed image.

- [16] A. Subramaniam, D. Yang, H. D. Yu, A. Nemiroski, S. Tricard, A. Ellerbee, S. Soh, and G. Whitesides, *Proc. Natl. Acad. Sci. USA* **111**(36), 12980–12985 (2014).
- [17] F. Iliovski, K. Mirica, A. Ellerbee, and G. Whitesides, *Soft Matter* **7**, 9113–9118 (2011).
- [18] K. Mirica, F. Iliovski, A. K. Ellerbee, S. Shevkoplyas, and G. Whitesides, *Adv. Mater.* **23**, 4134–4140 (2011).
- [19] Y. Yang, G. P. Lopez, and B. B. Yellen, *ACS Nano* **7**(3), 2705–2716 (2013).
- [20] G. Singh, H. Chan, A. Baskin, E. Gelman, N. Reprin, P. Král, and R. Klajn, *Science* **345**, 1149 (2014).
- [21] V. Lebedev and D. Weld, *J. Phys. B* **47**, 155003-1–155003-5 (2014).
- [22] A. Demirörs, P. Pillai, B. Kowalczyk, and B. Grzybowski, *Nature* **503**, 99–103 (2013).
- [23] L. Woldering, A. Been, L. Alink, and L. Abelmann, *Intermag 2014 Digest Book*, pp. 3164–3165 (2014).
- [24] M. Rycenga, J. McLellan, and Y. Xia, *Adv. Mater.* **20**, 2416–2420 (2008).
- [25] T. Clark, J. Tien, D. Duffy, K. Paul, and G. Whitesides, *J. Am. Chem. Soc.* **123**, 7677–7682 (2001).
- [26] W. Hertland and M. Hair, *J. Phys. Chem.* **75**, 2181–2185 (1971).
- [27] A. Awomolo, L. Jiang, J. Zhang, G. Jursich, and C. Takoudis, *J. Undergrad. Res.* **1**, 47–51 (2007).
- [28] R. P. Feynman, R. B. Leighton, and M. Sands, *The Feynmann Lectures on Physics, Volume II*, (Addison Wesley, Pearson 1964).
- [29] W. M. Haynes, Magnetic susceptibility of the elements and inorganic compounds, in: *CRC Handbook of Chemistry and Physics*, 94th edn. (CRC Press, 2013), pp. 4.131–4.136.
- [30] A. Winkleman, R. Perez-Castillejos, K. L. Gudiksen, S. T. Phillips, M. Prentiss, and G. M. Whitesides, *Anal. Chem.* **79**(17), 6542–50 (2007).
- [31] W. M. Haynes, Physical Constants of Inorganic Compounds List of Abbreviations, in: *CRC Handbook of Chemistry and Physics*, 94th edn. CRC Press, 2013), pp. 4.43–4.101.
- [32] K. A. Mirica, S. T. Phillips, S. S. Shevkoplyas, and G. M. Whitesides, *J. Am. Chem. Soc.* **130**(52), 17678–17680 (2008).
- [33] R. Ravaud, G. Lemarquand, S. Babic, V. Lemarquand, and C. Akyel, *IEEE Trans. Mag.* **46**(9), 3585–3590 (2010).
- [34] R. Hartley and A. Zisserman, *Multiple View Geometry in Computer Vision* (Cambridge University Press, Cambridge, New York, 2000).